geoconvention
Calgary • Canada • May 15-19 2017

Basis Pursuit for Seismic Spectral decomposition

Jiajun Han and Brian Russell*
Hampson-Russell Limited Partnership, CGG Geo-software, Canada

Summary

Spectral decomposition is a powerful analysis tool used to identify the frequency content of seismic data. Many spectral decomposition techniques have been developed, each with their own advantages and disadvantages. The basis pursuit technique produces a high time frequency resolution map through formulating the problem as an inversion scheme. This techniques differs from conventional spectral decomposition methods in that produces not only frequency information but also phase information. The synthetic and real data examples shown in this study illustrate the advantages of the basis pursuit method for seismic spectral decomposition.

Introduction

Spectral decomposition, also called time frequency analysis, has a wide range of applications in geophysics, especially in the area of seismic analysis. Its aim is to reveal signal features such as any underlying periodicities, which facilitates the seismic interpretation. Spectral decomposition has been utilized in a variety of applications such as hydrocarbon detection (Fomel, 2013), geological structure detection (Liu et al., 2011), stratigraphic delamination (Bonar and Sacchi, 2013) and attenuation estimation (Reine et al., 2012).

Spectral decomposition maps a 1D time signal into a 2D image of frequency and time, which describes how the frequency content varies with time. The widely used short time Fourier transform (STFT) calculates the fast discrete Fourier transform in each time window to compute the spectrogram. The window length of the STFT determines the trade-off between time and frequency resolution. To overcome this limitation, the continuous wavelet transform (CWT) was developed by Morlet et al. (1982a and b). Chakraborty and Okaya (1995) show the superiority of the CWT over the STFT in terms of spectral resolution. Likewise, the S-transform, proposed by Stockwell et al. (1996), can be interpreted as a hybrid of STFT and CWT.

Recently developed spectral decomposition techniques include methods like empirical mode decomposition, or EMD, (Han and Van der Baan, 2013), the synchrosqueezing transform (Herrera et al., 2014) and basis pursuit (BP) (Bonar and Sacchi, 2013). Although the mathematical foundations of these methods are different than the CWT, they all show huge improvement on the spectral resolution of the data. Tary et al. (2014) compare these methods with conventional methods such as the STFT, CWT and S transform on five benchmark signals, and comment that the recently developed techniques show clear improvements in most cases.

In this paper, we investigate the performance of the basis pursuit method. Instead of only focusing on the time frequency amplitude map, we will also investigate the phase information that can be obtained from basis pursuit. We first describe the theory of basis pursuit as applied to spectral decomposition. We then compare this technique with three conventional methods on a synthetic example. Finally, we use extend the basis pursuit attribute as an external attribute for predicting the porosity in the Blackfoot dataset from Western Canada.

Theory

The main principle behind basis pursuit (BP) is the decomposition of a signal into its individual components using a predefined dictionary (Chen et al., 2001). Unlike matching pursuit, BP is not a greedy alorithgm. It identifies all atoms and its accociated weights simultaneously into a single inversion problem.

A seismic trace $s(t)$ is represented as the convolution of a family of wavelets $\psi(t,n)$ and their accociated coefficients , $a(t,n)$ as

$$s(t) = \sum_{n=1}^{N} [\psi(t,n) * a(t,n)] \tag{1}$$

where N is the number of wavelets, t is time and n is the dilation of the wavelet determining its frequency (Tary et al., 2014). Using maxtrix notation, equation (1) can be rewritten as

$$\mathbf{s} = (\boldsymbol{\psi}_1\ \boldsymbol{\psi}_2\ ...\ \boldsymbol{\psi}_N)\left(\mathbf{a}_1\ \mathbf{a}_2\ ...\ \mathbf{a}_N\right)' + \eta = D\mathbf{a} + \eta \tag{2}$$

where $\boldsymbol{\psi}_N$ denotes the convolution matrix of $\psi(t,n)$, D is the wavelet dictionary, and η is the random noise. At this stage, $\mathbf{a}$ can be intrepretated as the time-frequency dependent refelectivity, which corresponds to the time frequency distribution of the seismic trace $\mathbf{s}$.

Equation (2) is an under-determined linear equation, the solution can be calculated through the least squares technique. Since high time frequenncy resolution is preferred, the sparsity of $\mathbf{a}$ can be controlled using the L1 norm. Therefore the cost function is

$$J = \frac{1}{2}\|\mathbf{s} - D\mathbf{a}\|_2^2 + \lambda\|\mathbf{a}\|_1 \tag{3}$$

The first term in J represents the data misfit term based on the the L2 norm, which is the least squares error between the obseved and predictied data. The second term in the cost function determines the number of nonzero coefficients in $\mathbf{a}$. The term λ is the trade-off parameter controlling the relative strength between the two terms. Various solvers exist for equation (3) , such as iterative reweighted least squares. We chose the fast iterative shrinkage thersholding algoithm (Beck and Teboulle, 2009) and implenmented it in the frequency domain to enhace the computation efficiency.

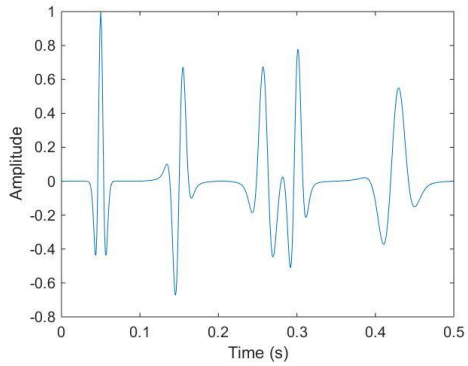

Figure 1: Synthetic example. The trace is composed of five Ricker wavelets. From left to right, the wavelets include: 60 Hz with zero phase, 40 Hz with 90 degree phase, 30 Hz with -45 degree, 40 Hz with 45 degree, and 20 Hz with 45 degree phase, respectively.

Examples

We first compare BP with the other three well-known conventional spectral decomposition methods on a synthetic data example. The synthetic example (Figure 1) is composed of five different Ricker wavelets of various frequency and phase characteristics. From left to right in Figure 1, they are: a zero phase, 60 Hz Ricker wavelet , a 90 degree phase rotated 40 Hz wavelet, , with a -45 degree rotated 30 Hz wavelet, a 45 degree rotated 40 Hz wavelet , and finally a 45 degree rotated 20 Hz Ricker wavelet.

The STFT, CWT and S transform algorithms generate reasonable amplitude results, as shown in Figures 2 (a), (b) and (c). The methods all discriminate the isolated Ricker wavelets well, but due to the spectral smear (Tary et al., 2014), these conventional methods can't distinguish the two closely spaced wavelets between 0.25s and 0.3s, and only show an asymmetric feature. BP performs the best when compared with the other methods (Figure 2(d)), and locates both the amplitude at an accurate time as well as the correct frequency, with the highest time frequency resolution.

Another benefit from BP is the phase information that can be obtained. The phase maps from STFT, CWT and S transform (Figure 3 (a), (b) and (c)) are hard to interpret, mainly due to the artefacts from spectral smearing. The BP phase map (Figure 3(d)) shows clean and clear features extracted from the synthetic data. By reading the values at the local maximum points, accurate phase information can be obtained. Note that a Ricker wavelet dictionary is selected as the predefined dictionary in the BP implementation shown here.

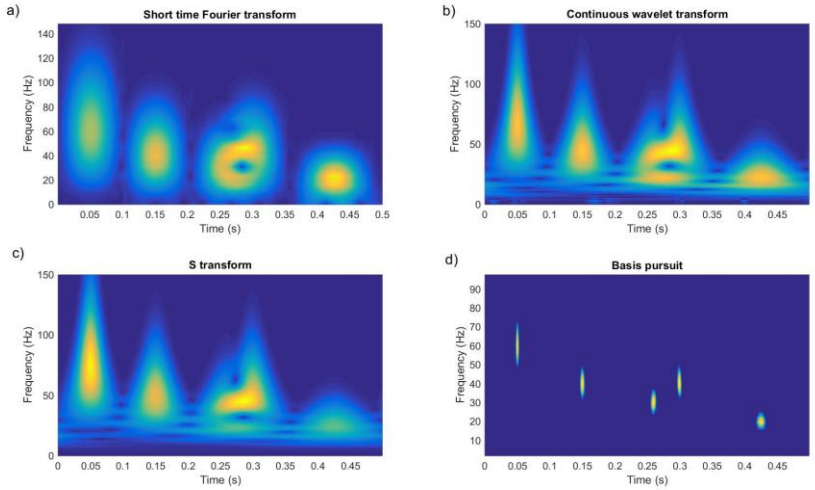

Figure 2: Time frequency amplitude map of the synthetic trace. (a). Short time Fourier transform. (b). Continuous wavelet transform. (c). S transform. (d). Basis pursuit.

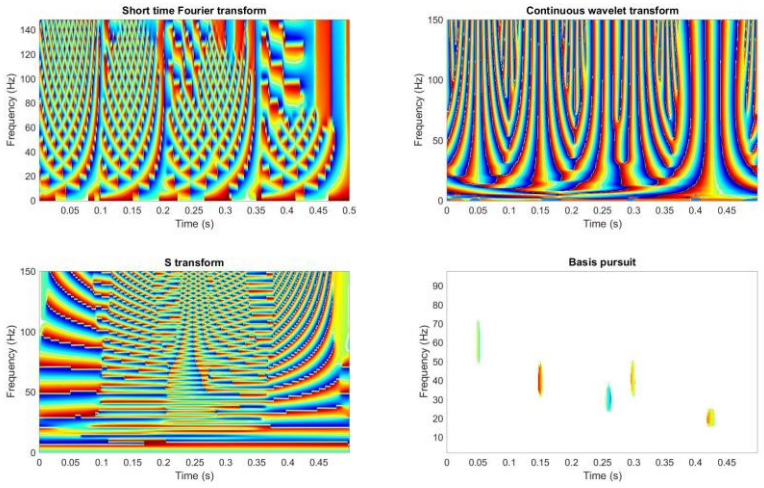

Figure 3: Time frequency phase map of the synthetic trace. (a). Short time Fourier transform. (b). Continuous wavelet transform. (c). S transform. (d). Basis pursuit.

To verify the phase information φ from Figure 3(d), we apply a phase rotation to the synthetic trace, using the equation $x_{rot}(\mathrm{t}) = \cos\phi\,\mathrm{x(t)} + \sin\phi\,\mathrm{H[x(t)]}$. ,with $x(\mathrm{t})$ the input trace, and $H[.]$ the Hilbert transform operator (van der Baan, 2008). The red trace in Figure 4 is the trace after the phase rotation, which is the zero phase signal.

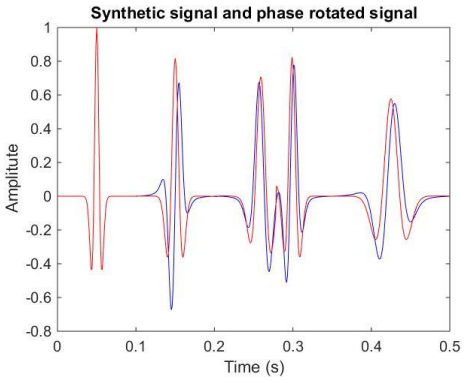

Figure 4: Blue trace is the original synthetic trace shown in Figure 1; the red trace is after phase rotation, which shows the zero phase signal feature.

Next, we apply the BP algorithm to the Blackfoot dataset, and the take the basis pursuit outputs as the external attributes for predicting the porosity. The seismic section is shown in Figure 5 view 1, on the left. The predicted porosity without using the basis pursuit attributes is shown in Figure 5 view 2, in the middle of the display., The correlation in the target zone is 79%, and the validation correlation is 49%. When the basis pursuit amplitude and phase attributes are included, as shown in the right panel of Figure 5, the application correlation and the validation correlation in the target zone are improved to 95% and 60%, respectively, and the predicted porosity shown in Figure 5 view 3 is much improved. View 3 discriminates the upper valley and lower valley features more clearly than the view 2, which are highlighted by the white circles. Note that the workflow for predicting the porosity is the EMERGE algorithm in the Hampson-Russell software package, and the prediction opotion is the probabilistic neural network (PNN).

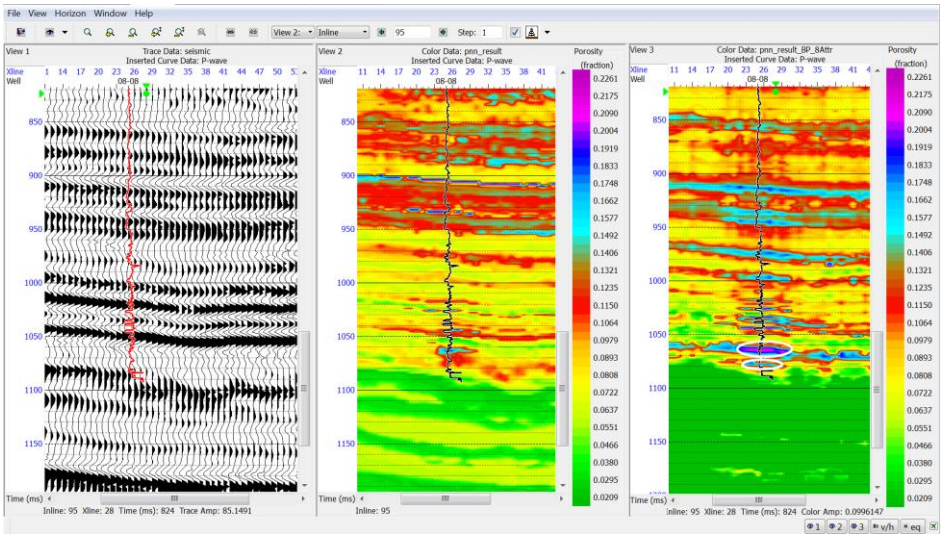

Figure 5: View 1: (left) seismic section. View 2: (middle) the predicted porosity without the basis pursuit attributes. View 3: (right) the predicted porosity using the basis pursuit attributes. The white circles highlight the key geological features.

Conclusions

In this paper we have demonstrated that the basis pursuit algorithm produces higher time frequency resolution than conventional methods of spectral decomposition, and that both amplitude and phase information can be accuarately calculated. The synthetic and real data examples shown here illustrate the improved performance found when using the basis pursuit method.

Acknowledgements

The author thanks Hampson-Russell Limited Partnership, CGG Geo-software for the permit to show the case data example.

References

Beck, A., Teboulle, M., 2009. A Fast Iterative Shrinkage-Thresholding Algorithm for Linear Inverse Problems. SIAM J. Imaging Sci. 2, 183–202.

Bonar, D., Sacchi, M., 2013. Spectral decomposition with f−x−y preconditioning. Geophys. Prospect. 61, 152–165.

Chakraborty, A., Okaya, D., 1995. Frequency-time decomposition of seismic data using wavelet-based methods. Geophysics 60, 1906–1916.

Chen, S., Donoho, D., Saunders, M., 2001. Atomic decomposition by basis pursuit. SIAM J. Sci. Comput. 43, 129–159.

Fomel, S., 2013. Seismic data decomposition into spectral components using regularized nonstationary autoregression. Geophysics 78, O69–O76.

Han, J., Van der Baan, M., 2013. Empirical mode decomposition for seismic time-frequency analysis. GEOPHYSICS 78, O9–O19.

Herrera, R.H., Han, J., Mirko, van der B., 2014. Applications of the synchrosqueezing transform in seismic time-frequency analysis. Geophysics 79, V55–V64.

Liu, G., Fomel, S., Chen, X., 2011. Time-frequency analysis of seismic data using local attributes. Geophysics 76, P23–P34.

Morlet, J., Arens, G., Fourgeau, E., and Giard, D., 1982a, Wave propagation and sampling theory – Part I: Complex signal and scattering in multilayered media: Geophysics, 47, p. 203-221.

Morlet, J., Arens, G., Fourgeau, E., and Giard, D., 1982b, Wave propagation and sampling theory – Part II: Sampling theory and complex waves: Geophysics, 47, p. 222-236.

Reine, C., Clark, R., Baan, M. Van Der, 2012. Robust prestack Q-determination using surface seismic data: Part 2—3D case study. Geophysics 77, B1–B10.

Stockwell, R.G., Mansinha, L., Lowe, R.P., 1996. Localization of the complex spectrum: the S transform. IEEE Trans. Signal Process. 44, 998–1001.

Tary, J.B., Herrera, R.H., Han, J., Baan, M. Van Der, 2014. Spectral estimation — What is new? What is next? Rev. Geophys. 52.

Van der Baan, M., 2008. Time-varying wavelet estimation and deconvolution by kurtosis maximization. Geophysics 73, V11–V18.